OPEN ACCESS SLAC-PUB-16770

Plasmon scattering probing of electronic states in diamond at extreme conditions

S. H. Glenzer,[1] L. B. Fletcher,[1] H. J. Lee,[1] M. J. MacDonald,[2,3] U. Zastrau,[4] M. Gauthier,[1] D. O. Gericke,[5] J. Vorberger,[6] E. Granados,[1] J. B. Hastings,[1] and E. J. Gamboa[1]

[1] *SLAC National Accelerator Laboratory, 2575 Sand Hill Road, MS 72, Menlo Park, CA 94025, USA*
[2] *SLAC National Accelerator Laboratory, 2575 Sand Hill Road, MS 72, Menlo Park, CA 94025 USA*
[3] *University of Michigan, 2455 Hayward St, Ann Arbor, MI 48109 USA*
[4] *High-Energy Density Science Group, European XFEL, Albert-Einstein-Ring 19, 22761 Hamburg, Germany*
[5] *Centre for Fusion, Space and Astrophysics, Department of Physics, University of Warwick, Coventry CV4 7AL, United Kingdom*
[6] *Institute of Radiation Physics, Helmholtz Zentrum Dresden-Rossendorf e.V., 01328 Dresden, Germany*

(Dated: July 8, 2016)

We measured the collective plasmon scattering spectrum from diamond at pressures approaching 370 GPa. Samples are dynamically compressed employing counter-propagating laser beams where the compression states are determined by Bragg scattering. X-ray energy loss spectroscopy with 8 keV photons from the Linac Coherently Light Source (LCLS) is then applied to probe the electronic state. The x-rays excite a collective interband transition, leading to a clear plasmon signal whose dispersion matches density functional theory. The data reveal a pressure-dependent Penn gap and demonstrate a non-conducting warm dense matter state for conditions of planetary interiors.

The extraordinary mechanical and optical properties of carbon are the basis of numerous technical applications [1] and make diamond anvil cells the premier device to explore the high-pressure properties of materials [2, 3]. In contrast, the behavior of carbon at the high pressure and moderate temperatures typically occurring in planetary interiors [4, 5] is poorly understood. Here, prediction for the boundaries between the different high-pressure phases, their microscopic structure, and the conductivity at high pressure carry large uncertainties. As there is growing evidence of the abundance of carbon in the interiors of several planets, these information are urgently needed for modelling planetary structures, their evolutions and the generation of the external magnetic fields. Moreover, the behavior of carbon under large pressures is also one of the major inputs for describing inertial confinement fusion experiments [6, 7], where an ablator made of high-density carbon rather than plastic has been shown to reduce the entropy in implosions [8].

One of the most important problems at high pressures is the closure of the band gap and the creation of a highly conducting, metallic phase (Mott transition). Although this is a general behavior, the transition point and the path towards this phase transition pose severe challenges for theoretical predictions [9]. Unlike for most semiconductors, both the direct and indirect band gaps of diamond have been predicted to first increase with compression [10, 11] before decreasing and eventually collapsing at extremely high pressures. *Ab initio* simulations have predicted a stable insulating phase under purely hydrostatic pressures of over 1 TPa [12, 13] and a band gap collapse at a combination of high uniaxial stresses >400 GPa and hydrostatic pressures of >100 GPa [14].

Indications for the unusual opening of the band gap only exists at very low pressures; measurements have been performed for pressures smaller than 10 GPa by static compression experiments [15, 16]. Conversely, a red shift of the absorption edge was observed at uniaxial pressures of over 300 GPa [17, 18]. However, until now it remains unknown whether this behavior is a consequence of the intrinsic closure of the diamond band gap, is related to the impurities in natural diamond, or comes from deformation of the highly strained anvils leaving considerable uncertainties about the pathway towards the Mott transition in carbon. The transition to a conducting fluid has been inferred for conditions under dynamic shock-compression, which is connected to a considerable temperature rise at several hundred GPa [19].

In this Letter, we present the first dynamic high-pressure experiments at LCLS that ramp-compress solid samples to pressure of 370 GPa. These conditions provide temperatures below 3000 K, close to the Neptune adiabat , and allow access of ultra bright x-ray probing [20]. We employ a unique combination of precision x-ray measurements of the electronic and ionic structure. The frequency shift of the inelastically scattered x-rays encodes the optical properties and, thus, the behavior of the band gap in the sample [21]. We observe an increasing direct band gap in diamond in well-characterized compression states from simultaneous x-ray diffraction. The scattering spectra show a clear signature of collective plasmon excitations that characteristically shifts to higher frequency losses with the increasing pressure. Combining these data with *ab initio* simulations reveals an opening of the band gap up to the highest observed pressures. Moreover, we can clearly rule out pressure-induced changes as a sources of the observed red shift of the optical absorption edge.

Our experiment was performed at the end station for Matter in Extreme Conditions (MEC) in the LCLS at the

This material is based upon work supported by the U.S. Department of Energy, Office of Science, Office of Basic Energy Sciences, under Contract No. DE-AC02-76SF00515.

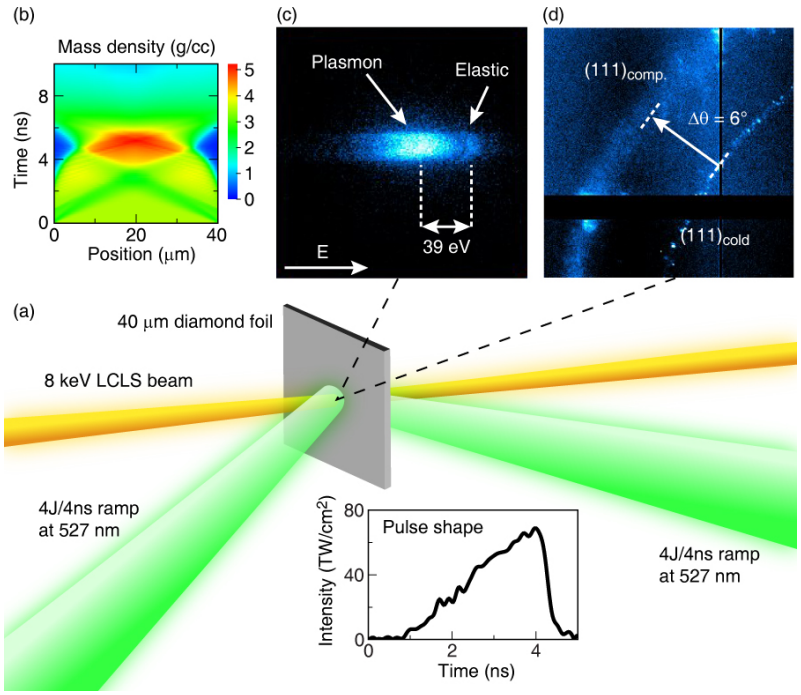

Figure 1. Configuration for dynamic-compression experiment. (a) The diamond foils are compressed with a high-energy optical laser and probed with the high-photon flux x-ray beam from LCLS. The scattered x-rays are resolved in spectrum and angle. (b) Hydrodynamic simulations predict a density of $5\,\mathrm{gcm}^{-3}$ when the compression waves collide. c) Data for the inelastic scattering spectrum showing a distinct plasmon resonance. d) The Debye-Scherrer rings in the diffraction images are sensitive to the density of the sample.

SLAC National Accelerator Laboratory [22]. Fig. 1(a) gives a schematic of the experimental setup. Thin foils of diamond, created by chemical vapor deposition, were heated and compressed by driving two counter-propagating pressure waves with intense optical lasers incident on each surface. Hydrodynamic simulations with the HELIOS code using the PROPACEOS equation of state tables [23] predict densities of up to $5\,\mathrm{g/cm}^3$ at the collision of the two compression waves several nanoseconds after the start of the laser drive (see Fig. 1(b)).

The diamond foils were prepared by chemical vapor deposition onto a silicon substrate seeded with a diamond powder. The samples were 3 x 3 mm at a thickness of 40 μm. The foil surfaces were analyzed using a profilometer showing an average grain size of 100 nm. The crystal grains show a typical preference to the orientation of the substrate planes [24]. The average density of the foils was measured using the profilometer and a microbalance as 3.45 g/cc. This is slightly less than the bulk density (3.51 g/cc) as measured by x-ray diffraction, which is explained by the formation of amorphous carbon at the boundaries of the crystal grains. The main impurity was hydrogen adsorbed on the surfaces of the grains at a content of 0.1% by mass as estimated by electron energy loss spectroscopy.

Compression of the sample was achieved by two optical lasers each delivered up to 4 J of light at 527 nm in a 4 ns long ramp pulse. The laser spots were smoothed with continuous phase plates giving a focal spot of 60 μm FWHM and a peak intensity of $70\,\mathrm{TW/cm}^2$.

The compressed samples were probed by 8 keV x-rays from the LCLS. The FEL beam provided a typical pulse energy of 0.3 mJ of x-rays on target and was focused to a spot size of 10 μm Thus, the central, most uniformly compressed region of the diamond sample was probed.

Forward scattering spectra from the compressed diamond were recorded at a fixed angle of $25\pm0.26^\circ$ using a highly oriented pyrolytic graphite crystal spectrometer. A Cornell-SLAC Pixel Array Detector observed Debye-Scherrer rings from x-ray diffraction over an angular range of $2\theta = 17\text{-}55^\circ$, sufficient to observe the (111) and (220) diffraction peaks. For each shot, we recorded inelastic spectra using a graphite crystal spectrometer as well as powder diffraction rings with an area detector in

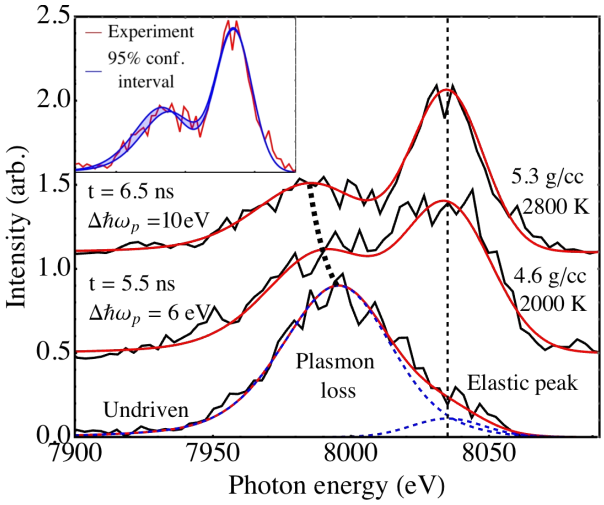

Figure 2. Scattered spectra from compressed diamond. The experimental data (black lines) preceding (5.5 ns) and at coalescence (6.5 ns) are compared to the synthetic spectra (red lines). The compressed shots show a downshift in the plasmon peak as compared to the undriven control sample. The blue dashed lines show the relative contributions to the scattering for the undriven spectrum, while the dashed line connects the centers of the plasmon peaks. Inset: the spectrum at 6.5 ns is compared to a 95% confidence interval for the fitted plasmon shift.

the forward direction [25]. Examples for these two kinds of spectra are shown in Fig. 1(c) and (d). The angular shift of the Bragg peaks in the compressed samples directly provides the density; the spectral shift of the plasmon peak is sensitive to the changes in the electronic structure.

Figure 2 shows examples of inelastic scattering spectra measured at times near the coalescence of the ramp waves, thus sampling different density states. For comparison, we also show a control spectrum from undriven diamond. A larger density from the compression leads to an increase in the plasmon loss. These changes are reflected in the experimental spectra by a greater shift of the inelastic feature away from the elastic peak. We determine the plasmon frequency shift by fitting a theoretical spectrum to the data, with the total plasmon loss as a free parameter. The plasmon peak is shifted by up to 10 ± 1 eV from the position of the uncompressed diamond.

Observing the energy-loss of scattered x-rays is a well-established technique in dynamic compression experiments which can yield the material properties of warm dense matter or plasma states [20, 26]. In this regime, inelastic scattering comes primarily from free electrons that have been ionized or reside in the conduction band. Under certain conditions, the response of the electrons becomes collective and plasmons are observed [21]. In static compressions experiments, such plasmons have also been measured with recent results from sodium at pressures up to 100 GPa [27].

A similar collective resonance can also be excited in insulators and semiconductors. Previous studies on nonmetals have almost exclusively characterized thin membranes using electron energy loss spectroscopy [28]. For dynamically compressed matter, where the high pressure and density state is maintained for only several nanoseconds, electron scattering will be insufficient. Here, only the advent of record-brightness LCLS x-ray free electron laser provides a near ideal probe, permitting single-shot measurements of the inelastic x-ray scattering spectrum.

Valence electrons localized within chemical bonds in insulators can be collectively excited into an available conduction band. For diamond, the four sigma bonds then oscillate between bonding and anti-bonding states. The plasmon and average separation between these two bands, the Penn gap, form a system of coupled oscillators. The resonance frequency for a scattered wave vector $\mathbf{k}$ may be modeled as

$$\omega(\mathbf{k}) = \sqrt{\omega_b^2 + \omega_{\mathrm{Penn}}^2} + \frac{\hbar^2}{m_e}\alpha\,\mathbf{k}^2\,. \qquad (1)$$

Here, $\omega_b = n_b e^2/m_e\epsilon_0$ is the plasma frequency associated with the valence electrons with density n_b, and ω_{Penn} is the Penn gap frequency [29] between the valence and conduction bands. The additional quadratic dispersion term goes beyond the usual Drude model and is introduced following the behavior of the random phase approximation for free electrons. We have measured the empirical dispersion constant α to be 0.22.

Taking $\omega_b = 31.1\,\mathrm{eV}$ from the valance electron density and $\omega_{\mathrm{Penn}} = 13.8\,\mathrm{eV}$ gives a plasmon loss of 34 eV for diamond under standard conditions [30, 31]. Under compression, the plasmon loss will shift to lower energies from both the densification and band gap opening. Thus, by independently constraining the density, we can experimentally determine the behavior of the band gap.

We compare the measured plasmon shift to predictions in Fig. 3(a). Here, we first assumed a constant Penn energy. The increase of the electron density due to the compression is not sufficient to explain the data. The remaining increase of the plasmon energy must be attributed to an increase of the Penn gap. To improve our modeling, we also use Penn gaps that have been extracted from density functional theory (DFT) simulations. The DFT calculations predict an increase in the Penn gap under compression which, when inserted into Eq. (1), gives an excellent agreement with the measured plasmon shift.

The experimental data indicate an increase in the Penn gap from 13.8 eV at normal density to 20.5 eV at the maximum compression of $5.3\,\mathrm{gcm}^{-3}$. Concomitant with the increasing Penn gap, the DFT simulations reveal a widening optical band gap. The calculated pressure coefficient is approximately 5 meV/GPa for pressures up to 80 GPa, 3meV/GPa up to 250 Pa, and then 2meV/GPa

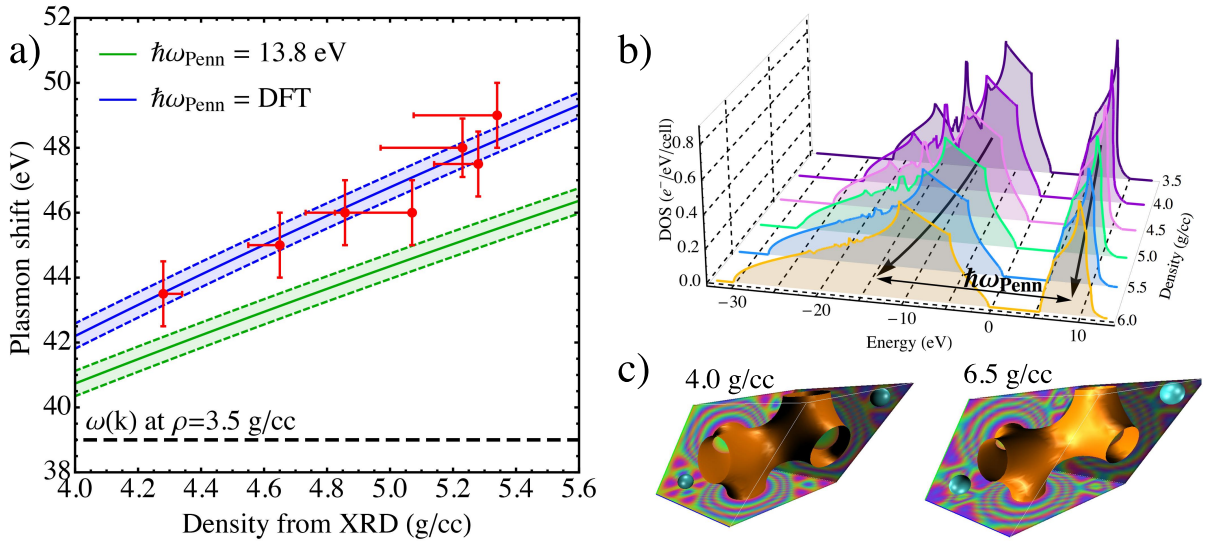

Figure 3. Analysis of the inelastic scattering data. (a) Measured plasmon shift versus density. The experimental data is compared to the two predictions using a constant band gap (green) and one inferred from DFT calculations of the density of states (blue). The density for the markers showing the experimental data is determined from the (111) diffraction peak with error bars inferred from the (220) peak. The dashed black line shows the plasmon shift of undriven diamond. (b) Density of states from the DFT calculations for different densities showing an opening of the band gap and modifications of the shape under compression. The arrows demonstrate the increase in the Penn gap with density. c) Simulated isosurfaces of the valence electron density of diamond. Under compression the bound electrons move closer to the ions, widening the band gap and stiffening the material.

to the highest simulated pressure of 800 GPa. These lowest pressure coefficients are comparable to previous theoretical and experimental work: 5 meV/GPa from the theoretical calculations by Fahy et al. [11], 6 meV/GPa from the experiments of Onodera et al. [16] to 2.3 GPa, and 6.9 meV/GPa at up to 7 GPa from Trojan et al. [15]. The stiffening of the band structure at high pressures demonstrates that the material properties cannot be inferred from extrapolation from low pressure studies.

At elevated temperatures, thermal ionic motion can lead to a reduction in the band gap [32]. By observing the intensity of the elastically scattered peak, we measured the temperature of the diamond sample through the Debye-Waller factor. The relative increase in the elastic peak yields a maximum temperature of 2800 K [33], which has a negligible impact on the DFT results.

Under the large anisotropic stresses, typical of diamond anvil cells [34], the band gap of diamond has been predicted to collapse at pressures of 400 GPa [35]. As our maximum inferred pressure is close to this value, it is important to consider non-hydrostatic effects that compress the lattice differently along each direction and may lead to a disagreement in the lattice constants, and thus density for different Bragg peaks. By measuring the shifts of the (111) and (220) diffraction peaks, we find the largest strain in our experiment results in a 0.03 Å anisotropy in the inferred lattice constants and an error of 5% in the density. Our DFT calculations show that this small amount of strain has only negligible effects on the band structure. These small strains are in strong contrast to the 10% elongation of the lattice constant as predicted in highly strained diamond anvils [35].

In conclusion, we present the first detailed measurements combined with DFT simulations of the electronic structure of diamond at extreme pressures. For that goal, we have transformed electron loss spectroscopy into the x-ray domain allowing probing of larger samples on much shorter time scales. By employing wavelength- and angularly-resolved x-ray scattering simultaneously, we show that diamond remains an insulator to densities of at least 5.3 gcm^{-3} and pressures of 370 ± 25 GPa. We have observed the band gap of diamond to increase under compression. The stability of diamond under strong hydrostatic compression can have large implications for carbon-rich planets as a pressure-induced metallic phase has significantly different thermodynamic properties. Moreover, our results point to anisotropy and impurities as a source for the closure of the optical window in diamond anvil cells.

This work was performed at the Matter at Extreme Conditions (MEC) instrument of LCLS, supported by the DOE Office of Science, Fusion Energy Science under contract No. SF00515. This work was supported by DOE Office of Science, Fusion Energy Science under FWP 100182. The target work was supported by a Laboratory Directed Research and Development grant. UZ was supported by the Peter Paul Ewald Fellowship of the VolkswagenStiftung.

[1] Nazare, M. H. & Neves (Eds.), A. J. *Properties, Growth and Applications of Diamond* (Institution of Engineering and Technology, 2000).

[2] Jayaraman, A. Diamond anvil cell and high-pressure physical investigations. *Rev. Mod. Phys.* **55**, 65–108 (1983). URL http://link.aps.org/doi/10.1103/RevModPhys.55.65.

[3] Mao, W. L. *et al.* Bonding changes in compressed superhard graphite. *Science* **302**, 425–427 (2003).

[4] Hubbard, W. *et al.* Interior structure of neptune: comparison with uranus. *Science* **253**, 648–651 (1991).

[5] Fortney, J. *et al.* Frontiers of the physics of dense plasmas and planetary interiors: Experiments, theory, and applications. *Physics of Plasmas (1994-present)* **16**, 041003 (2009).

[6] Lindl, J. D. *et al.* The physics basis for ignition using indirect-drive targets on the national ignition facility. *Physics of Plasmas (1994-present)* **11**, 339–491 (2004).

[7] Lindl, J. *et al.* Review of the national ignition campaign 2009-2012. *Physics of Plasmas (1994-present)* **21**, 020501 (2014).

[8] MacKinnon, A. *et al.* High-density carbon ablator experiments on the national ignition facilitya). *Physics of Plasmas (1994-present)* **21**, 056318 (2014).

[9] Kremp, D., Schlanges, M. & Kraeft, W.-D. *Quantum statistics of nonideal plasmas*, vol. 25 (Springer Science & Business Media, 2006).

[10] Goñi, A. R. & Syassen, K. Optical properties of semiconductors under pressure. *Semicondt. Semimet.* **54**, 247–425 (1998).

[11] Fahy, S., Chang, K. J., Louie, S. G. & Cohen, M. L. Pressure coefficients of band gaps of diamond. *Phys. Rev. B* **35**, 5856 (1987).

[12] Yin, M. T. & Cohen, M. L. Will diamond transform under megabar pressures? *Phys. Rev. Lett.* **50**, 2006–2009 (1983). URL http://link.aps.org/doi/10.1103/PhysRevLett.50.2006.

[13] Yin, M. T. Si-iii (bc-8) crystal phase of si and c: Structural properties, phase stabilities, and phase transitions. *Phys. Rev. B* **30**, 1773–1776 (1984). URL http://link.aps.org/doi/10.1103/PhysRevB.30.1773.

[14] Nielsen, O. H. Optical phonons and elasticity of diamond at megabar stresses. *Phys. Rev. B* **34**, 5808–5819 (1986). URL http://link.aps.org/doi/10.1103/PhysRevB.34.5808.

[15] Trojan, I. A., Eremets, M. I., Korolik, M. Y., Struzhkin, V. V. & Utjuzh, A. N. Fundamental gap of diamond under hydrostatic pressure. *Jpn. J. Appl. Phys.* **32**, 282 (1993). URL http://stacks.iop.org/1347-4065/32/i=S1/a=282.

[16] Onodera, A. *et al.* Pressure dependence of the optical-absorption edge of diamond. *Phys. Rev. B* **44**, 12176–12179 (1991). URL http://link.aps.org/doi/10.1103/PhysRevB.44.12176.

[17] Vohra, Y. K., Xia, H., Luo, H. & Ruoff, A. L. Optical properties of diamond at pressures of the center of earth. *Appl. Phys. Lett.* **57**, 1007–1009 (1990).

[18] Mao, H.-K. & Hemley, R. Optical transitions in diamond at ultrahigh pressures. *Nature* **351**, 721–724 (1991).

[19] Bradley, D. K. *et al.* Shock compressing diamond to a conducting fluid. *Phys. Rev. Lett.* **93**, 195506 (2004). URL http://link.aps.org/doi/10.1103/PhysRevLett.93.195506.

[20] Fletcher, L. *et al.* Ultrabright x-ray laser scattering for dynamic warm dense matter physics. *Nature Photonics* **9**, 274–279 (2015).

[21] Glenzer, S. H. & Redmer, R. X-ray thomson scattering in high energy density plasmas. *Rev. Modern Phys.* **81**, 1625 (2009).

[22] Glenzer, S. *et al.* Matter under extreme conditions experiments at the linac coherent light source. *Journal of Physics B: Atomic, Molecular and Optical Physics* **49**, 092001 (2016).

[23] MacFarlane, J. J., Golovkin, I. E. & Woodruff, P. R. Helios-cr–a 1-d radiation-magnetohydrodynamics code with inline atomic kinetics modeling. *J. Quant. Spectrosc. Radiat. Transfer* **99**, 381–397 (2006).

[24] Dawedeit, C. *et al.* Grain size dependent physical and chemical properties of thick cvd diamond films for high energy density physics experiments. *Diamond Relat. Mater.* **40**, 75 – 81 (2013).

[25] Gauthier, M. *et al.* New experimental platform to study high density laser-compressed matter. *Rev. Sci. Instrum.* (2014).

[26] Glenzer, S. H. *et al.* Observations of plasmons in warm dense matter. *Phys. Rev. Lett.* **98**, 065002 (2007).

[27] Mao, H. K. *et al.* Electronic dynamics and plasmons of sodium under compression. *Proc. Natl. Acad. Sci. U.S.A.* **108**, 20434–20437 (2011).

[28] Egerton, R. F. Electron energy-loss spectroscopy in the tem. *Reports on Progress in Physics* **72**, 016502 (2009). URL http://stacks.iop.org/0034-4885/72/i=1/a=016502.

[29] Penn, D. R. Wave-number-dependent dielectric function of semiconductors. *Phys. Rev.* **128**, 2093 (1962).

[30] Ferrari, A. C. *et al.* Density, sp 3 fraction, and cross-sectional structure of amorphous carbon films determined by x-ray reflectivity and electron energy-loss spectroscopy. *Phys. Rev. B* **62**, 11089 (2000).

[31] Robertson, J. Diamond-like amorphous carbon. *Mater. Sci. Eng. R* **37**, 129–281 (2002).

[32] Romero, N. A. & Mattson, W. D. Density-functional calculation of the shock hugoniot for diamond. *Phys. Rev. B* **76**, 214113 (2007).

[33] Gamboa, E. J. *et al.* Single-shot measurements of plasmons in compressed diamond with an x-ray lasera). *Physics of Plasmas* **22**, – (2015). URL http://scitation.aip.org/content/aip/journal/pop/22/5/10.1063/1.4921407.

[34] Ruoff, A. L., Luo, H. & Vohra, Y. K. The closing diamond anvil optical window in multimegabar research. *J. Appl. Phys.* **69**, 6413–6416 (1991).

[35] Surh, M. P., Louie, S. G. & Cohen, M. L. Band gaps of diamond under anisotropic stress. *Phys. Rev. B* **45**, 8239 (1992).